Potential for External Reinforcement of Insulated Rail Joints

M.Gallou[1], B.Temple[1], C.Hardwick[1], M Frost[2], A.El-Hamalawi[2]

[1]LB Foster Rail Technologies UK

[2]Loughborough University

Corresponding Author: Maria Gallou, Research Engineer

LB Foster Rail Technologies (UK) Ltd, Stamford Street, Sheffield, S9 2TX

Email: MGallou@lbfoster.com

Abstract

This paper aims to investigate alternative ways of reducing the deterioration and failure of railway track insulated rail joints (IRJs). Joints deteriorate faster than rail initially due to the structural discontinuity present. This weakness results in both extra displacement as a consequence of applied load and the dynamic force that results as a consequence. Over time this situation worsens as the impacts and applied stresses both damage and soften the ballast and supporting subgrade under the joint. This study initially presents a static finite element model designed to simulate the mechanics of IRJs and a comparison between plain rail and a suspended insulated rail joint under various support stiffnesses. Product design options of reinforced IRJs are then chosen as input variables of the model. Results of the model are compared with field and laboratory data acquired via the Video Gauge, which is a new high-resolution optical measurement technique. Results show that the use of strap rails or more robust I-beam sections in the vicinity of the IRJ to stiffen the support structure can significantly reduce the displacement and the subsequent dip angle seen at an IRJ. This potentially presents a means of improving the IRJ behaviour. Their impact becomes more significant for soft support conditions. Although these results are indicative for new IRJ conditions, field measurements indicate that the magnitude of deflection of IRJs is a result of the structural discontinuity of the rail, the dynamic P2 force, the wheel condition, the degraded ballast and it significantly increases with time under repeated load. Thus, it is recommended that careful field implementation and testing will indicate the effect of an external enhancement on the timely degradation of insulated rail joints.

Keywords

Rail joint, Insulated rail joint, dipped joint, modelling, reinforcement, track

1 INTRODUCTION

The railway system's dependability is based on the rail components' structural integrity. The failure of insulated rail joints (IRJs) is a worldwide problem in railway networks and a major component of the maintenance cost. The mechanical failure of an IRJ can increase ballast degradation, and can also impede the electrical integrity of an IRJ thereby causing train detection issues (signalling). IRJs are considered a weak point because of the discontinuity in the stiffness of rail. The main aim of this study was to investigate the effect of external enhancement in the performance of IRJs as a strategy of improved performance of the jointed track. IRJs deflect more than regular plain track because of the lower cross section area, lower section moment of inertia of the fishplate and the elasticity of the insulation layer. This structural discontinuity interacting with the wheel impact load causes a vicious cycle of joint and track degradation. With the passage of a single wheel over the joint, joint anomalies such as bolt looseness and rail height mismatches are caused and with repeated wheel passage rail end wear occurs. The degraded joint provokes large deflections and amplifies the dynamic force induced at the joint.

This leads to the acceleration of the track degradation, which in turn provokes a progressive increase on the joint deflection. It was hypothesised by the authors that structural reinforcement of the track structure in the vicinity of the joint could reduce the initial deflection increment to less than or equal to that of the plain rail. Thus the damage cycle can be reduced. This was shown in this paper by finite element (FE) modelling validated by field measurements using high-precision optical equipment. This paper starts with a literature review describing the mechanics of an insulated rail joint, current track deflection field measurement techniques and previous modelling of IRJs. The accuracy of Video Gauge for measuring the performance of IRJ is evaluated using laboratory testing, then field measurements of plain rail and IRJ are presented. The methodology includes an implicit static finite element model to investigate the effect of structural changes and stiffness on the deflection of standard plain track and of IRJs. The parameters used include the selection of sleeper type, sleeper spacing, stiffness per sleeper end, material properties of rail, fishplate, railpad and endpost, and type of external structural strengthening for a suspended IRJ. As model outputs, rail deflection and dip angle of the IRJ were evaluated. A comparison was conducted between the FE model and the field data, followed by a discussion of the results.

1.1 Mechanics of IRJ

The main purpose of a rail joint is to separate electrical circuits in rails and turnouts whilst joining two pieces of rail where continuously welded rail is not possible. This is achieved through the use of joint bars (fishplates), fastened through the web of the rail with bolts. Insulated rail joints (IRJs) are critical components of railway signalling infrastructure where sections of track are separated into separate blocks so track circuits to be used for train detection. While a purely mechanical bolted joint just comprises fishplates and bolts, an IRJ includes material fitted between the rail ends made of a non-conductive material (endpost) as well as an insulated lining to separate the fishplates from the rails all to maintain electrical separation of the adjoining rails (see Figure 1). Sometimes IRJs are also glued to increase joint robustness.

Although the fishplates are designed to offer a similar shear capacity to the parent rail section they support, a bolted joint arrangement remains weaker in resistance to bending. As a consequence, rail joints deflect more than adjacent continuous rails on nominally the same support conditions. This also means that an increased dynamic force is generated as a wheel passes over the joint and over time, a ballasted support structure will accrue more damage and the deflection at a joint is usually found to progressively increase until maintenance limits are reached or failure occurs.

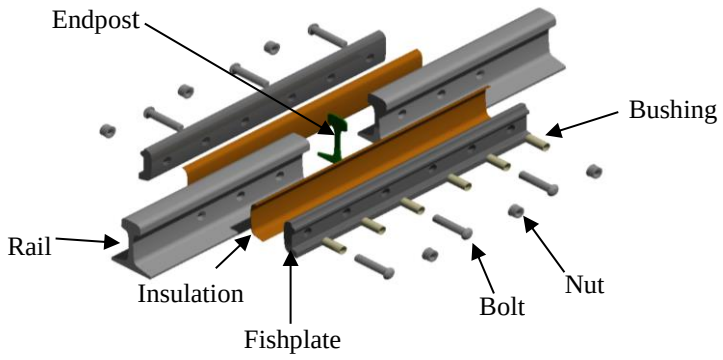

Figure 1. View of IRJ assembly (amended from [1])

In a standard UK fishplated joint, the moment of inertia of the joint fishplates is only 29% of that of the parent rail [2]. This stiffness discontinuity results in around 90% of the bending moment being transferred across the joint [3]. This can be improved by modifying the design of the joint or the support conditions; however the weakness in bending is still present. In addition it has been found that the dynamic impact from wheel in a rail joint is three times larger than the static wheel load [4]. The service of the rail joints varies depending on the traffic loading and frequency; Australian research has claimed that it can be only 50 MGT of freight traffic [5]; American research has claimed 200 MGT with replacement requirements in a period of 12-18 months with costs of $10,000 per mile per year [4], which is significantly less than the service life of other rail components that withstand up to 1000 MGT [6], whereas failures of IRJ cost Network Rail (UK) £10 millions in a two year period [7].

An IRJ can fail mechanically, electrically or both. Mechanical (structural) failure occur either in the fishplates, rail, bolts or epoxy [8] due to high static, dynamic and fatigue loads that weaken or cause the total failure of rail joint components. Electrical failure is caused when the electrical isolation between the two adjoining rails is lost and can be caused either by a mechanical failure or by other factors such as lipping or contamination.

Additional to the vertical, longitudinal and lateral forces applied in the track system [9, 10], the P2 force represents the total vertical force from the combined static gravity load on the wheel and dynamic force from the unsprung masses due to any variations in the alignment of the rail including vertical track irregularities such as a rail joint.

P2 forces can cause rapid deterioration of track quality. Key parameters for its calculation are the train speed, the size of the defect, the track stiffness, the bending stiffness of the rail and the mass of the rail and the wheelset. A maximum permissible value of P2 has been defined at 322 kN (static load + dynamic increment) for a defined defect angle of 20 mrad [11].

1.2 Previous experimental testing of IRJ

The evaluation of IRJ performance in the laboratory and in the field has been assessed in the past by strain gauges and impact load detectors [1, 4, 12-15]. Results included time histories of bending, shear, lateral shear strains and wheel-rail forces. The literature shows that no work has been conducted in measuring the displacements of rail joints and interpretation of the IRJ displacement in relation to the plain rail and underlying support stiffness or structure. For this reason measurement techniques exploited for track deflection will be applied to identify IRJ deflection.

1.3 Review of current track deflection field measurement techniques

A wide range of techniques have been used in the past decade to measure the deflection performance of railway track during the passage of a train. The following methods have been identified [16]:

- Linear variable displacement transducers (LVDT) [17]
- Geophones [18]
- Laser deflectometer [19]
- Remote video monitoring using PIV and DIC [20]

1.4 The Video Gauge

In this paper the Video Gauge (VG), previously used only once [21], is used for real-time in-situ high resolution measurements. It is based on Digital Image Correlation (DIC) principles and Video Extensometry (VE). DIC is based on pattern recognition techniques and image pixel tracking. VG exploits sub-pixel pattern recognition algorithms that enable ultra-high resolution measurements of displacement, strain and rotation to be made. It supports the use of multiple cameras for 2D or 3D measurements. Frame by frame comparison allows for measurement of deflections. The VG system enables data of high quality and quantity and offers substantial time and cost saving when compared with traditional instrumentation sampling [16]. Frequencies, higher than any other technique (up to 300 Hz) can be reached whereas sampling frequencies more than 300 Hz can be achieved by using expensive higher frame rate cameras.

The suitability of the VG for measuring sleeper and rail modules has been shown in the past [22], but never for measuring rail joints. For the purposes of this research the efficacy and accuracy of the VG for measuring rail joints in the field was evaluated first by laboratory measurements (see 2.1 Laboratory validation section).

1.5 Modelling of IRJs

Most Finite Element Modelling (FEM) of IRJs [23-25] comprises FEM of the ratchetting (plastic strain accumulation) in the rail head edges at the discontinuity between the rail ends in the case of a mechanical or an insulated rail joint. Recommendations have been restricted to fishplate and endpost material/size optimisation for improved rail joint performance. Rail deflections and stresses in the epoxy layer with different sleeper and fishplate dimensions with centred and off-centred loading have been investigated [26]. Maximum rail displacements were found in a range of 1.7-3.1 mm. Few authors have looked at the problem from a holistic point of view by looking at the impact of the track support structure on a rail joint. The range of maximum rail deflection for continuous rail was presented at 1-3.3 mm (0.13 in) and 1.1-4.3 mm (0.17 in) for a suspended IRJ for various support conditions [27]. Finally, it was recently shown by a 2D vehicle-track model that the impact force P1 that is mostly causing the track degradation due to the accordance of frequencies with those of the track, is greatly influenced by the joint angle, the mass of the rail and the mass of the wheelsets, whereas the peak force P2 is mainly affected by the support stiffness at the joint angle apart from the mass of the wheelset and the railpad stiffness [28].

In the past the track deflection for various wheel loads and track conditions have been measured. The range of rail displacements measured varies for different measurement techniques, different types of track and trains. For example, 1-7 mm of rail deflection has been measured with PIV video cameras, LVDTs and geophones [18, 29]. Filtered rail displacements of post-processed geophones output data have been found lower than absolute values from video techniques. A range of 2 -10 mm of rail displacement has been identified for gap sizes 0 -30 mm between the sleeper and the ballast (for singular or multiple unsupported sleepers). Perfect track has been found to deflect in a range of 1.5 - 3 mm whereas degraded ballasted track has been measured to deflect up to 10 mm [29]. Nevertheless, little work has been conducted into the effect of the support structure on the displacement of IRJs. The majority of previous studies have been focused in experimentally measuring the impact wheel forces and strains in IRJs for validating FE models aiming to reduce the localised rail fatigue (plastic strain) by looking at micro scale at the rail joint, whereas the IRJ degradation is progressively increasing due to the increased damage to the underlying structure. IRJs displacements have been evaluated only by numerical models (1 - 4.5 mm for

various track conditions) [26, 27]. There is no current literature showing the effect of structural enhancement of the performance of rail joints by using numerical modelling of joints compared to plain track validated with accurately assessed field displacements.

2 EVALUATION OF PLAIN RAIL AND RAIL JOINT DISPLACEMENTS

The applicability of Video Gauge (VG) for measuring IRJs was validated in the laboratory. The deflection increment of IRJs was evaluated in both laboratory and field conditions in order to validate the numerical model.

2.1 Laboratory validation

A 4-bolt standard (wedge fit) glued IRJ, rail joint (CEN 60) of 3 m length was tested in a four-point bend under cyclic loading at a frequency of 1 Hz. The joint endpost was centrally positioned between two vertical hydraulic actuators, (separation distance 600 mm) and applied a synchronised vertical cyclic force onto the rail. The displacement was recorded by the VG at a frequency 66.36 Hz from a distance of 800 mm using a lens of 16 mm focal length. This resulted in a horizontal field of view 550 mm giving a resolution of 3.7 pixels/mm. A LVDT was also positioned on top of the endpost for comparison with the VG values in order to check the accuracy of the VG. The loading used (120 – 404 kN) exceeds the maximum static wheel load on UK infrastructure (25 tonne axle load) and approximates the vertical dynamic force generated by the static wheel load and low frequency dynamic [P2] forces based on recent research [2]. Figure 2 shows a comparison between the LVDT and the VG data. The excellent correlation of the results indicated that the Video Gauge was successful in measuring accurately the complex dynamic deflection histories of plain rail and rail joint.

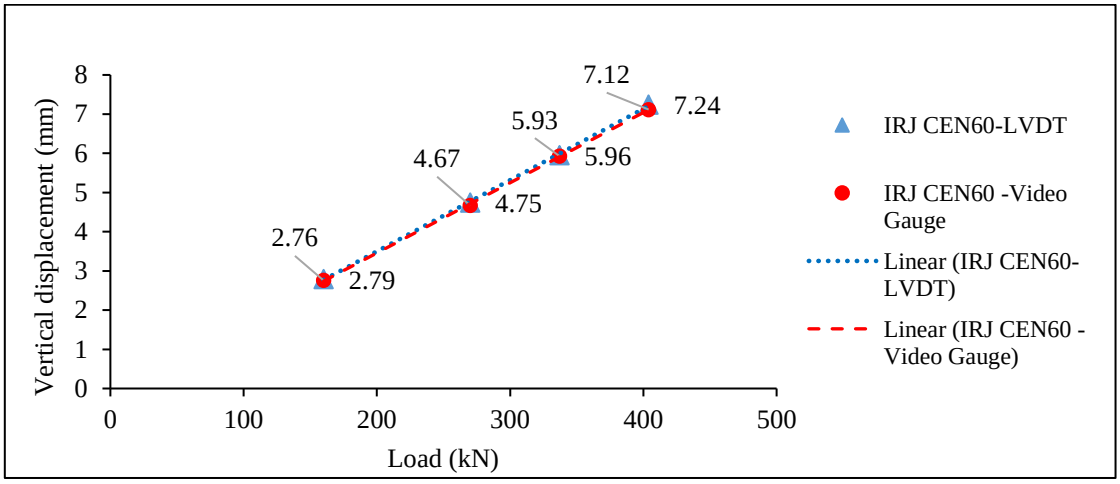

Figure 2: Comparison between Video Gauge and LVDT displacement values for IRJ CEN 60 at varying load cases

2.2 Field measurements

The deflection of a 6-bolt rail joint and the adjacent plain rail were measured on a live railway line at Winsford (UK). Two high speed cameras were used recording at 75 fps from a distance 5.5 m. Lenses of focal length 75 mm and 50 mm were used in order to provide a field of view of 2 m. Five different passenger trains were measured, (two Desiro and three Pendolino type trains). From the time history, the speed of each train was calculated. The Desiro trains are lighter (11 tonnes axle load, observed speed 57 - 115.5 mph) than Pendolino trains (15 tonnes

axle load, observed speed 125 mph). Figure 3 shows a typical time-displacement plot during the passage of an 11-car Pendolino at 125 mph. Each vehicle consists of 4 axles. The positive displacement is uplift of the rail, ahead of or behind the wheels. By taking into account the maximum displacement value captured for each train, a displacement trace of each measurement point was plotted (see Figure 4). Distance is measured horizontally (x=0 m) from the centre of the IRJ along the parent rail.

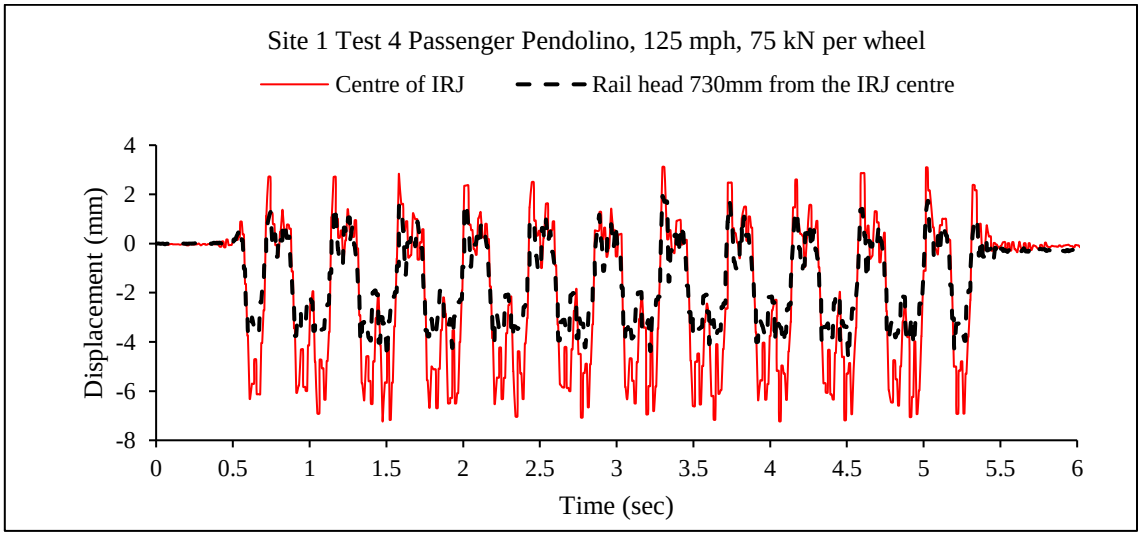

Figure 3. Time-displacement plot. Comparison between IRJ and rail due to passage of passenger train at 125mph.

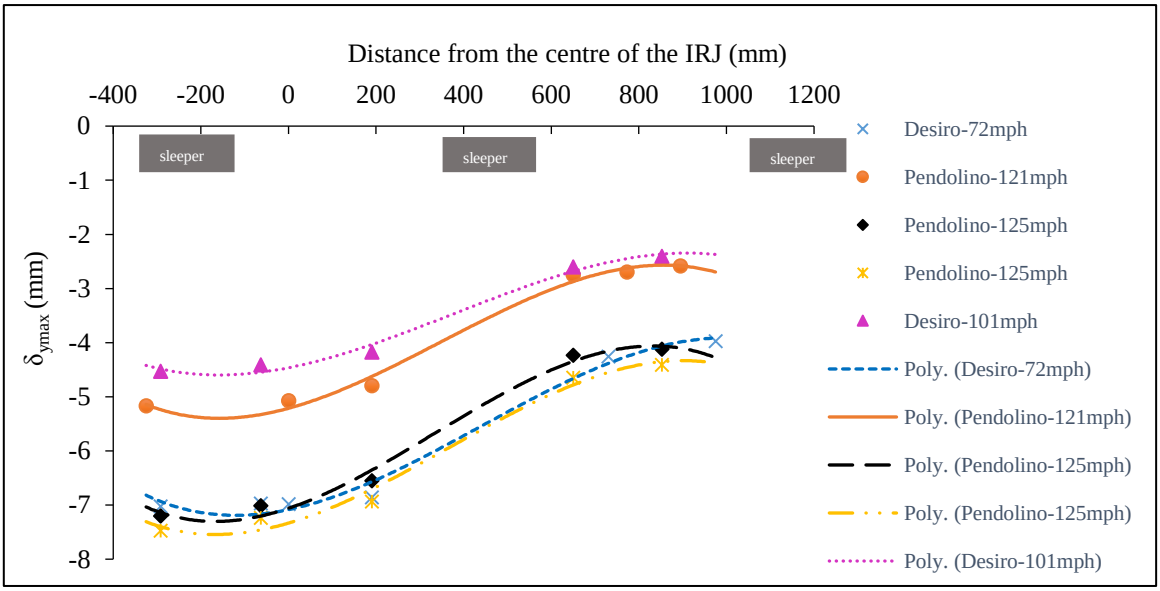

Figure 4. Maximum displacements of rail head at various distances from the centre of the IRJ,

By looking at the results, it can be seen that there are local differences in the field measured displacements. This can be attributed to three main causes; firstly the fact that absolute maximum displacement values have been plotted rather than an average or RMS value of all peak values around a wheel passage; secondly the fact that the sampling frequency (75 Hz) may not be adequate to capture the maximum deflection at the train speed; thirdly the wheel impact and the existence of potential wheel flats in some trains may have caused an increase in the P2 force, increasing the resulting displacement. For this reason the comparison between the averages of peak

displacements for each wheel between three different train types and speeds for the two track positions is presented in Table 1. The results presented are typical of other tests of IRJs undertaken at other site locations under similar train speeds. Differences between trains of similar axle load are attributed to wheel impact factors.

Table 1. Comparison of average of peak displacements between centre of IRJ and plain track 730mm away from the IRJ for various trains and speeds.

Average of peak vertical displacements (mm)		
Position	Plain rail	IRJ centre
Distance from the centre of IRJ	730 mm	0 mm
Pendolino at 125 mph	3.86	6.58
Desiro at 101 mph	2.36	4.23
Desiro at 72 mph	3.28	5.8

The table shows typical plane rail displacements between 2.36 and 3.86 mm and larger joint deflections of 4.23 to 6.58 mm as would be expected. The values agree with the literature.

3 FINITE ELEMENT ANALYSIS (FEA) MODEL

A numerical model was created that represent the plain track and the rail joint deformations. A basic plain rail model was first constructed for the appropriate track geometry. An investigation of the appropriate track length to be simulated was conducted and a ten-sleeper long track was selected as optimal after looking at the load distribution pattern. The sleeper deformation was investigated in an initial phase with different types of underlying support stiffness. The plain track model was compared with a model that included a rail joint in the middle of the track length. Reinforcement with strap rails was investigated in plain track before being applied to the same model with an IRJ added. By varying the underlying support stiffness, the model was used to show the effect of structural changes in the track deflection.

ANSYS Mechanical was used to perform 3-dimensional linear static structural analysis. All components of the track assembly were modelled as solid bodies. Table 2 describes the material properties assigned to the different components. The FE model included two CEN 56 rails of moment of inertia 2320.0 cm^4 (length 6500 mm) in a length of ten sleepers (see Figure 5). The sleeper spacing was 650 mm and track gauge was 1435 mm. The rails are sitting on rail pads of 10 mm thickness of medium stiffness 150 kN/mm. An endpost of thickness 6 mm made of polyurethane was used as insulation layer between the rails with a joint. Fishplate of length 914 mm and sectional area A=3967.77 mm^2, used in 6-bolt IRJs, was used. Bonded contact was applied between all components except the rail-endpost interface where frictional contact with a coefficient 0.2 was applied. Concrete G44 sleepers were used with the appropriate geometry [30]. "*Monoblock sleepers are always packed over an area on either side of the centre of the rail and ideally there should be no pressure between the sleeper soffit and the ballast in the concrete section*" [3]. For this reason the effective length of 500.1 mm at each side of the bottom surface of the sleeper was used for the ballast pressure that is equal to Lp=(L-c)/2, where L is the sleeper length and c the rail seat spacing. The support stiffness caseswas applied through spring elements in the effective length in both sides of the load position. Three support stiffness cases of 30, 115 and 200 kN/mm were investigated in

an initial modelling phase assessed from recent literature [31, 32]; further cases with degraded support stiffness or sand 15 kN/mm were subsequently added. A minimum dynamic sleeper support stiffness of 30 kN/mm per sleeper end has been defined for a renewed trackbed and of 60 kN/mm for a new trackbed [9]. A single static 125 kN force was applied in the vertical direction on the centre of each rail (see Figure 5). The load represents the maximum UK static load in UK track infrastructure. The load was applied in all cases as a pressure in the centre of the railhead. The load application area was selected by taking into account the ellipsoidal area of a wheel –rail contact patch according to the Hertz theory and after mesh optimisation. The plain rail was modelled for single load in the mid-span between two sleepers allowing comparison with the suspended IRJ. Body meshing with 5 mm element size was applied in the endpost and in the rail section adjacent to the joint (622 mm on both sides of the endpost). A refined meshing (see Figure 5) with maximum element size 30 mm was applied in the four supporting sleepers around the joint. (Note, in this study the elastic linear behaviour of the railpad controls partially the rail uplift whereas the spring behaviour of the rest of the fastening system was not considered as critical for the structural evaluation of the IRJs.) The bolt/bonded interface was not of direct interest as the IRJ was not tested to destruction. Bolt connections can trigger failure in degraded joints but the aim in the model was to simulate joints in a non - degraded state. Elastic constitutive law was used as the induced stresses due to the static load are not in excess of yield limits. Thus, material behaviours beyond yield were not of interest and an elasto-plastic failure criterion was not needed.

3.1 Model variables

Table 3 presents the cases modelled: a) plain track, b) suspended IRJ (SUS-IRJ), suspended IRJ enhanced with strap rails (SR SUS-IRJ), d) suspended IRJ strengthened with beams (BS SUS-IRJ). The reinforcing strap rails are rail sections with second moment of area I=2320 cm^4 positioned on top of the four central sleepers surrounding the IRJ. The reinforcing effect of a larger steel beam section with second moment of area I=3227 cm^4, (39% stiffer of that of the strap rail) and of a size that can fit in the track geometry was also evaluated (see Figure 6 and Figure 7). Outputs of deflection rail dip angle and strain were produced.

Table 2. Material properties in the FEA model

Material properties					
Component	Material	Stiffness	Modulus of Elasticity	Poisson's ratio	Density
		k	E	v	ρ
Rail/Fishplate	Structural steel		200 GPa	0.3	7850 kg/m^3
Railpad		150 MN/m	38.265 MPa	0.3	300 kg/m^3
Sleeper	Concrete		30 GPa	0.18	2300 kg/m^3
Endpost	Polyurethane		20.7 MPa	0.3	1200 kg/m^3

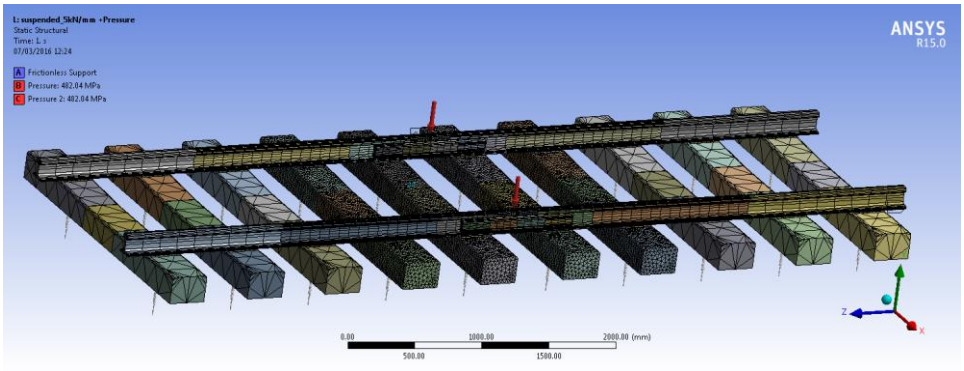

Figure 5. Geometry and meshing of the FEA model

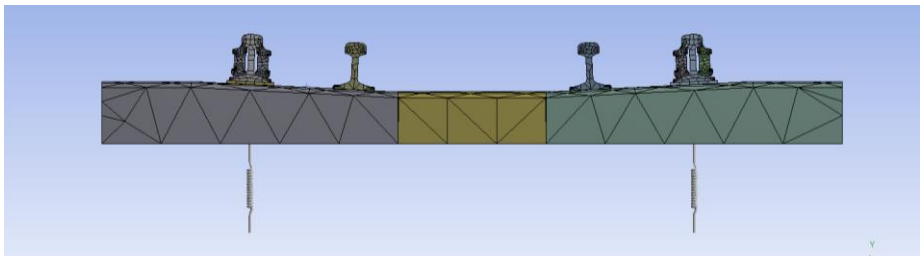

Figure 6. IRJ strengthened with strap rails FEA model

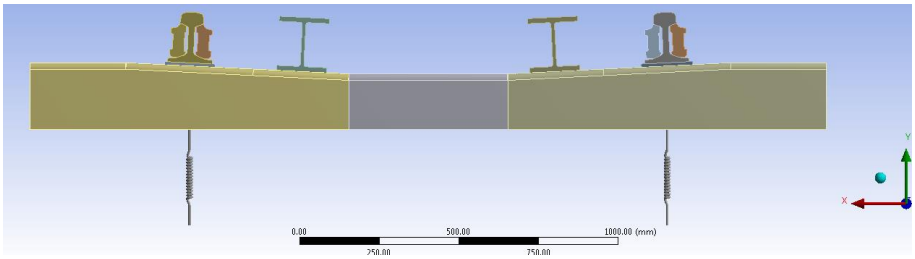

Figure 7. IRJ strengthened with I beams FEA model

Table 3. Parametric study cases

Configuration	Sleeper type	Second moment of area of enhancement	Stiffness per sleeper end (kN/mm)
Plain track	Concrete		5, 15, 30, 115, 200
Suspended IRJ (SUS-IRJ)	Concrete		5, 15, 30, 115, 200
Suspended IRJ enhanced with strap rails (SR SUS-IRJ)	Concrete	I_{xx}=2320 cm^4	5, 15, 30, 115, 200
Suspended IRJ strengthened with I beams (BS SUS-IRJ)	Concrete	I_{xx} =3227 cm^4	5, 15, 30, 115, 200

3.2 Verification of compressive stress on the rail head

The maximum Von-Mises stress on the rail head for the SUS-IRJ for the case of support- stiffness 30 kN/mm per sleeper end was measured to 1157.7 MPa. This value correlates with the values (1000-1250 MPa) found in the literature [23-25].

3.3 Model correlation with experimental data

From the FEA model of plain rail for the stiffness case of 30 kN/mm per sleeper end the maximum deflection in the rail head was measured at 2.13 mm (see Table 4). This correlates with the plain rail deflection measured by the VG in the laboratory at 120 kN (2.32 mm). Field measurements for plain rail gave a range of values 2.36 mm-3.86 mm for load cases 55-75 kN (see Table 1). The soft (degrading) support conditions reducing from 30 kN/mm until 5 kN/mm per sleeper end gave a range of rail vertical deflections between 2.13 mm and 6.78 mm respectively. (Note, the supporting stiffness can vary on site depending on the trackbed quality underneath each measuring point. In addition, the existence of voids in the interface of sleepers and ballast can cause non-uniformity in the rail deflection under same type of soil.) VG measurements gave a range of 4.23 mm to 6.58 mm for IRJ deflections in the field for varying speeds and train types. The FE model showed that a suspended IRJ deflects from 2.67 mm until 8.03 mm for support stiffnesses 30 kN/mm until 5 kN/mm. The agreement between the experimental and numerical data shows the validity and robustness of the FE model to validate its suitability for further investigation on IRJs effects under various wheel loads.

The verified FE model was then developed further to identify the effect of track structural changes on the IRJ deflection.

4 FEA RESULTS

A typical deformation plot of the suspended IRJ with reinforcing strap rails is illustrated in Figure 8. Figure 9 illustrates the typical displacement plot for the suspended IRJ for various support stiffnesses. Table 4 shows the maximum deflection and the calculated dip angle for each case. The effect of strap rails and I beam strengthening on the displacement and dip angle of the suspended IRJ under varying stiffness is shown in Figure 10 and Figure 11 respectively.

The dipped rail joint is taken into account in numerical models as a form of wheel–rail irregularity. An effective length of 500 mm on either side of dip is projected as the effective length of the irregularity of a dipped rail joint [33] . This is different to what industry considers; the effective length for the angle of the dipped RJ measurement is 125 mm on each side [3].

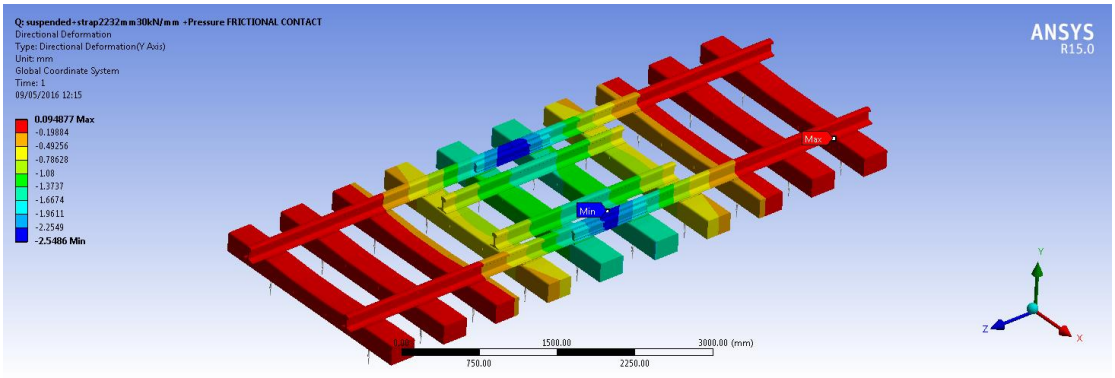

Figure 8. Deformation of suspended IRJ enhanced with strap rails (SR SUS-IRJ) with 30 kN/mm support stiffness per sleeper end

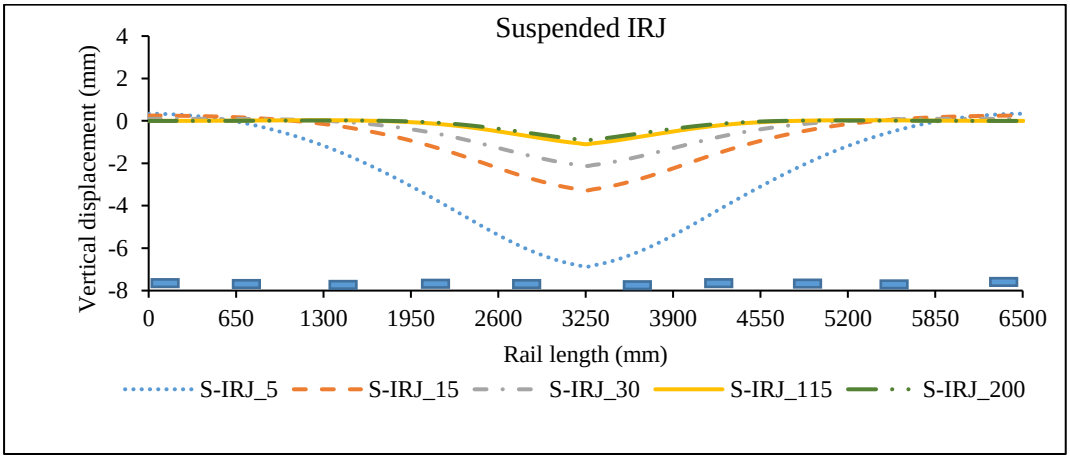

Figure 9. Deformation of suspended IRJ with stiffness variation

Table 4. Deformation results for plain rail and IRJs modelled for varying support stiffness

Stiffness per sleeper end (kN/mm)	200	115	30	15	5
	Maximum vertical displacement (mm)				
Plain rail	0.93	1.11	2.13	3.26	6.78
SUS-IRJ	1.28	1.49	2.67	3.97	8.03
SR SUS-IRJ	1.22	1.42	2.45	3.57	7.01
BS SUS-IRJ	1.19	1.38	2.37	3.45	6.8
	Total dip angle (mrad)				
SUS-IRJ	3.57	3.72	4.31	4.79	5.88
SR SUS-IRJ	3.5	3.61	4.04	4.35	5.04
BS SUS-IRJ	3.37	3.47	3.84	4.11	4.7

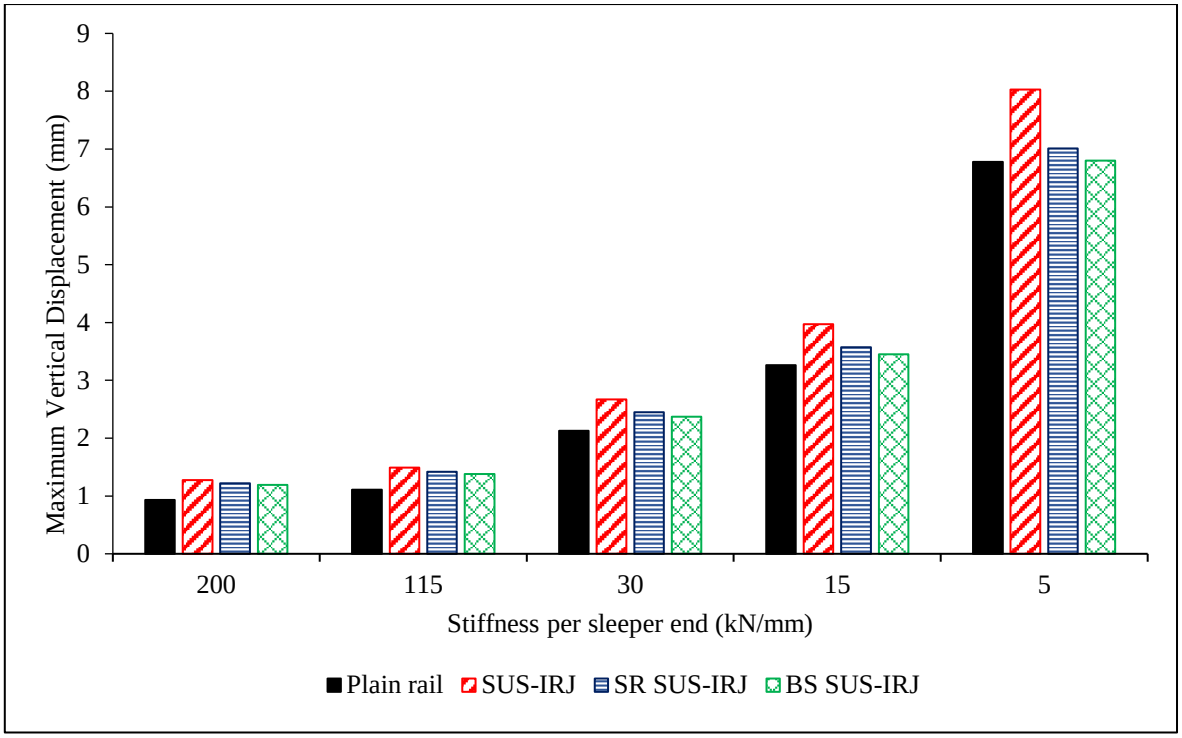

Figure 10. Effect of reinforcement on displacement of suspended IRJ for varying support stiffness

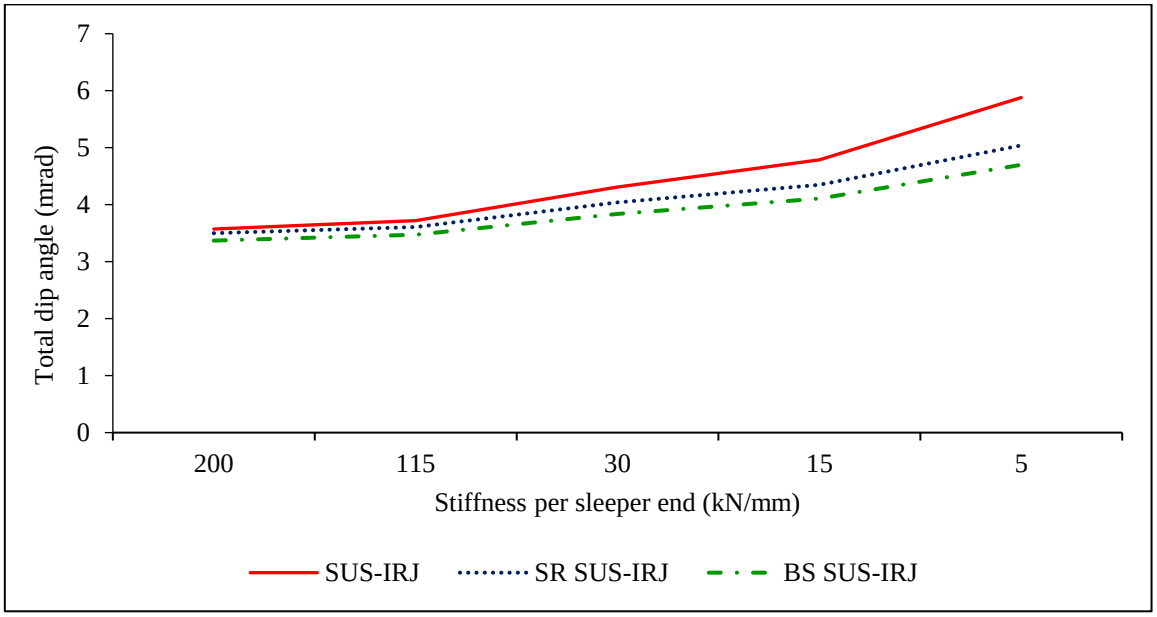

Figure 11. Effect of enhancement on total dip angle of suspended IRJs

5 DISCUSSION OF RESULTS

Both laboratory and field measurements verify that the rail joint deflects more than plain rail. The order of magnitude of the VG measured plain rail deflections are in agreement with literature review findings [18, 20, 29]. A comparison between the FEA results of plain rail and SUS-IRJ with the field measurements is depicted in Figure 12. The FE model was run with a wide range of support stiffness to capture the likely range of support conditions seen in the field. The soft support conditions from 30 kN/mm until 5 kN/mm per sleeper end gave a range of rail

vertical deflections between 2.13 mm and 6.78 mm respectively showing comparability. The actual stiffness of the track substructure layers in the field is not known so a comparison of the absolute values cannot be made.

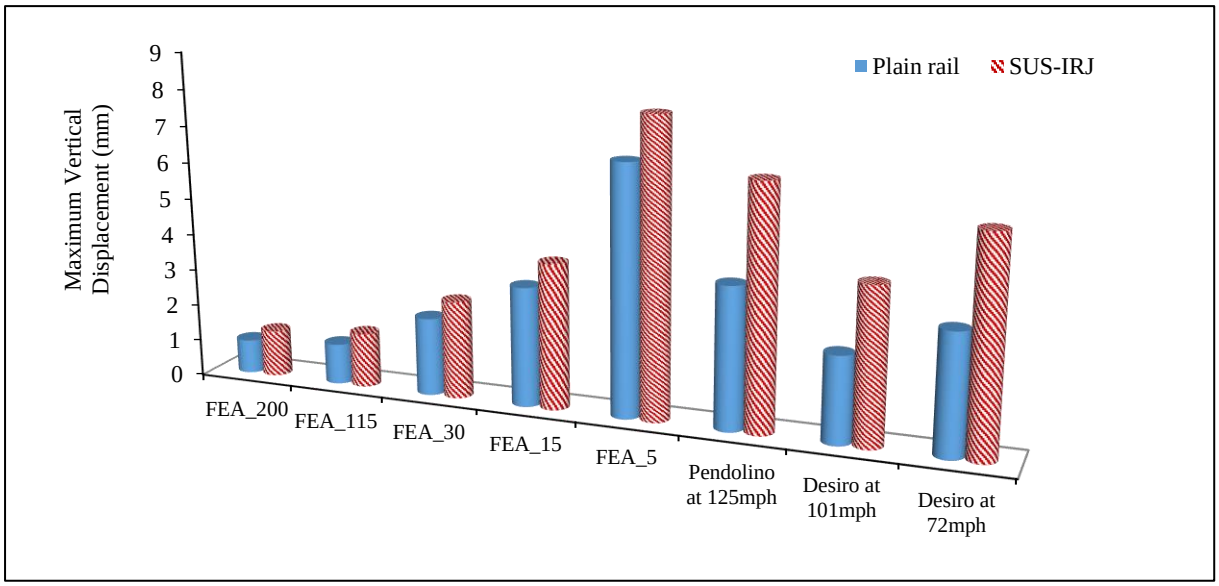

Figure 12. Comparison between FEA models and field deflection data for plain rail and SUS-IRJ.

The magnitude of FEA IRJ deflections are in agreement with previous research [26, 27]. All FE models showed that the deflection of a SUS-IRJ varies depending on the support stiffness. They proved that the additional deflection in a IRJ compared to that of a reference rail is lower when the model includes uniform support stiffness along the rail length whereas this increases with the degradation of the track underneath the joint. The current study investigated the effect of uniform degraded track support whereas the stiffness of a discrete number of sleepers underneath the joint was altered in other research [27].

An interpretation of the FE study indicated that the softer the support conditions, the higher the additional deflection an IRJ accumulates compared to that of a reference rail. However the relationship between the deflection increase and the stiffness decrease is not linear. For the case of 30 kN/mm per sleeper end, the SUS-IRJ deflects 25% more than the plain rail with a difference of 0.54 mm. For softer support conditions (15 kN/mm) the additional deflection is 0.71 mm whereas the difference decreases for stiff support conditions. The FE model gave a range from 2.67 to 8.03 mm for the deflection of a suspended IRJ for a support stiffness decreasing from 30 to 5 kN/mm that is in good agreement with the VG field data 4.23-6.58 mm. By taking into account the higher degradation rate of the ballast beneath an IRJ due to the cycle of deterioration of an IRJ and track conditions (due to the dynamic amplification of the wheel load at the joint) increased dynamic deflections can be found in the field. It should be noted that discrete ineffective support conditions in FEA (gaps in sleeper–ballast) interface in discrete sleepers underneath the IRJ) could increase the IRJ deflection.

In addition to the displacement, the dip angle of the suspended IRJ was calculated from the FE model for an effective length of 125 mm from each side of the centre of the IRJ [3]. This ranged from 3.57 mrad to 5.88 mrad for stiffness 200 kN/mm to 5 kN/mm per sleeper end (see Figure 11). The total dip angle was calculated from the VG field data for a number of cases. The values 1.26 - 4 mrad were found for speeds 57 – 125 mph. The dynamic

P2 forces were calculated as 58.5 - 108.4 kN and the load factors P2/F wheel were calculated to the range of 1.1 - 1.45. The numerical data are close to the field data that further validates the FE model.

The numerical model indicates that the dip angle for the SUS-IRJ increases at a lower rate than that of the displacement under independent support in a non –linear relationship. For 50% decrease in the support stiffness (from 30 kN/mm to 15 kN/mm per sleeper end) the maximum displacement of a SUS-IRJ increases 49% (from 2.67 mm to 3.87 mm) whereas the dip angle 11% (from 4.31 mrad to 4.79 mrad). For more degraded support conditions by altering the support stiffness from 15 kN/mm to 5 kN/mm the maximum displacement is doubled from 3.97 mm to 8.03 mm whereas the dip angle increases 23%. The magnitude of total dip angle of non -degraded IRJs that was used as input in previous research ranges from 1 to 14 mrad, and it has been assessed experimentally using various dip lengths from 0.1 m to 1.4 m [34]. By using the P2 force equation [11], the P2 force changes linearly with the static load, the speed and the dip angle and non- linearly with the track stiffness [34]. This means that by using the same equation the dip angle correlates non- linearly with the track stiffness as the current study indicates.

The effect of strap rail is greatest for the softer support conditions and less for stiffer support conditions. The strap rails decrease the deflection of the SUS-IRJ by 8% in the case of 30 kN/mm support. The SR SUS-IRJ deflects 15% more than the plain rail at 30 kN/mm, 9.5% more than the plain rail at 15 kN/mm, and 3% more than the plain rail at 5 kN/mm. However, the SR SUS-IRJ deflections are still higher than the deflections of plain rail for all support cases (Figure 10).

The strap rail reinforcement has a significant impact on the total dip angle. The rails decrease the total dip angle of the SUS-IRJ by 6% for the standard support-stiffness case (30 kN/mm), 9% for medium support conditions 15 kN/mm and 14% for softer support conditions (5 kN/mm) as shown in Table 4. This range follows the rate of displacement decrease due to strap rail enhancement.

The use of two standardised steel I beams has a higher effect on the improvement of the SUS-IRJ performance due to the 39% higher second moment of area. The BS-SUS IRJ deflects 11% less than the SUS-IRJ and 11% more than the plain rail for of 30 kN/mm support. For the softer support stiffness (15 kN/mm) the BS SUS-IRJ deflects 13% less than the SUS-IRJ and 6% more than the plain rail. The use of specific steel beams (that can easily be found in the steel industry) can improve the IRJ performance but could constitute a more expensive solution. The beam strengthening decrease the total dip angle 11% for 30 kN/mm/sleeper end, 20% for very soft conditions (5 kN/mm) whereas its effect is less significant for the stiff support. These relationships are depicted in Figure 11. These results clearly show the deflection can be reduced and life expectancy of joints can be increased by use of an external reinforcement.

Further investigation of the fastening system is required in order for such a beam to be connected to timber or concrete sleepers. In contrast, strap rails can be easily connected to timber sleepers through specific spikes. Precast concrete sleepers already exist in the rail industry with a fastening system in the required position for adding strap rails. The fact that the strap rails are already simply used in the rail industry in several cases such as transition zones, switches and in expansion joints facilitates the simple field implementation of a reinforced IRJ into the rail industry’s specifications, as the additional load they transfer into the sleepers has been previously approved.

6 CONCLUSIONS

A validated static numerical model capable of simulating plain rail and IRJ responses such as displacements, and total dip angle was created. The model was used to evaluate if external structural strengthening can reduce the deflection, and hence the deterioration level of an IRJ, so that the progressive deterioration in time of the ballast beneath the joint can be avoided.

The conclusions are summarised as follows:

- IRJs deflect more than plane rail and lead to increased local rates of trackbed degradation.
- The deflection of an IRJ is influenced measurably by the support conditions and by the dynamic increment of the generated P2 force regarding the speed and vehicle characteristics. The train type and the axle load affect the deflection.
- The decrease of deflection does not have a linear correlation with the stiffness increase.
- Use of strap rails reduces the deflection of a suspended IRJ. This improvement still makes the suspended IRJ deflect more than the plain rail. However, the strap rails are recommended as a cost-effective external reinforcement for maintaining the IRJ performance over time.
- Use of 39% stiffer I-beam sections reduces the deflection of a suspended IRJ to a greater level than that achieved by strap rails. More robust beams can lower the deflection of IRJ to a level similar to that of plain rails.
- The effect of external reinforcement on the reduction of displacement and dip angle of an IRJ is more critical for soft support conditions.
- The structural strengthening reduces the total dip angle of a suspended IRJ for all support conditions by a significant level.
- The total dip angle has not a linear correlation with the stiffness increase.

ACKNOWLEDGEMENTS

The author(s) wish to thank EPSRC for providing funding through the Centre for Innovative Construction Engineering (CICE) at Loughborough University and LB Foster Rail Technologies (UK) Limited for funding and supporting this research project.

REFERENCES

1. Soylemez E, Ciloglu K. Influence of Track Variables and Product Design on Insulated Rail Joints. *Transp Res Rec J Transp Res Board*. 2016 Jan;2545:1–10. 1.
2. Beaty P. *Experimental Testing Procedures to Investigate and Improve Insulated Rail Joint Design and Life Cycle*. MSc Thesis, University of Sheffield, UK; 2014.
3. Cope GH. *British Railway Track: Design, construction and maintenance*. 6th ed. Cope GH, England: Permanent Way Institution; 2001.
4. Akhtar M, O' Connor T, Davis D. Revenue service evaluation of advanced design insulated joints. In: *AREMA 2008 Annual Conference*, Salt Lake City, Utah, USA, September 21-24 2008.

5. Dhansekar M, Bayissa W. Review of Insulated Rail Joints. Report, CRC for Rail Innovation, R3.100; 2009.
6. Zarembski AM, Euston TL, Palese JW et al. Use of track component life prediction models in infrastructure management. In: *AusRAIL PLUS 2005*, Sydney, Australia, 22-24 November 2005.
7. Beagles AE, Beaty P, Fletcher DI et al. Insulated rail joint enhancement: testing and analysis. In: *Institution of Mechanical Engineers*. *The Stephenson Conference: Research for Railways*, London, UK, 21-23 April 2015.
8. Charlton ZI. *Innovative Design Concepts for Insulated Joints*. MSc Thesis, Faculty of Virginia Polytechnic Institute and State University; 2007.
9. GC/RT5021:2011. Railway Group Standard. Track System Requirements.
10. BS EN 1991-2:2011. Traffic loads on bridges.
11. GM/TT0088:1993. Permissible Track Forces for Railway Vehicles.
12. Askarinejad H, Dhanasekar M. Minimising the failure of rail joints through managing the localised condition of track. In: *Railway Engineering Conference 2015*, Edinburgh, UK, 30 June-1 July 2015.
13. Askarinejad H, Boyd P, Dhanasekar M. On-Track Testing of Insulated Rail Joints. Report No R3.100 (Previous BT17), CRC for Rail Innovation, Queensland University of Technology, Australia; 4 May 2011.
14. Askarinejad H, Dhanasekar M, Cole C. Assessing the effects of track input on the response of insulated rail joints using field experiments. *Proc Inst Mech Eng Part F J Rail Rapid Transit*. 2012 Sep 13;227 (2):176–87.
15. Bandula-Heva TM, Dhanasekar M, Boyd P. Experimental Investigation of Wheel/Rail Rolling Contact at Railhead Edge. *Exp Mech*. 2012 Dec 11;53 (6):943–57.
16. Gallou M, Temple B, Hardwick C, Frost M, El-Hamalawi A. Applicability of Video Gauge for the assessment of the track displacement. In: *The Stephenson Conference: Research for Railways*, London, UK, 25-27 April 2017.
17. Zakeri JA, Abbasi R. Field investigation on variation of rail support modulus in ballasted railway tracks. *Lat Am J Solid Struct*. 2012;9:643–56.
18. Bowness D, Lock A, Powrie W, Priest J, Richards D. Monitoring the dynamic displacements of railway track. *Proc Inst Mech Eng Part F J Rail Rapid Transit.* 2007 Jan 1;221 (1):13–22.
19. Innotrack. *Methods of track stiffness measurements*. Report, RSSB, Report no.TIP5-CT-2006-031415; 2006.
20. Murray C. *Dynamic monitoring of rail and bridge displacement using digital image correlation.* Master Thesis, Department of Civil Engineering, Queen's University, Kingston, Ontario, Canada; 2013.
21. Liu X, Markine V, Shevtsov I. Dynamic experimental tools for condition monitoring of railway turnout crosisng. *The Second International Conference on Railway Technology: Research, Development and Maintenance*, Ajaccio, Corsica, France; 8-11 April 2014.
22. Waterfall P, Temple B, Hardwick C, Sharam J, Plumb A. Video Measurement techniques for understanding wheel- induced lateral forces and track component deflections. *The Stephenson Conference-Research for Railways*. London, UK; 21-23 April 2015.

23. Mandal NK, Peach B. An Engineering Analysis of Insulated Rail Joints : A General Perspective. *Int J Eng Sci Technol.* 2010;2(8):3964–88.
24. Sandström J, Ekberg A. Numerical study of the mechanical deterioration of insulated rail joints. *Proc Inst Mech Eng Part F J Rail Rapid Transit*. 2009 May 1;223(3):265–73.
25. Zong N, Wexler D, Dhanasekar M. Structural and Material Characterisation of Insulated Rail Joints. *Electron Jourrnal Struct Eng*. 2013;13(1):75–87.
26. Himebaugh AK. *Finite Element Analysis of Insulated Railroad Joints*. MSc Thesis, Virginia Polytechnic Institute and State University; 2006.
27. Carolan ME, Jeong DY, Perlman AB. Engineering studies on Joint bar integrity, Part II: Finite element analyses. *Joint Rail Conference 2014*, Colorado Springs, Colorado, USA, 2-4 April 2014.
28. Grossoni I, Iwnicki S, Bezin Y et al. Dynamics of a vehicle-track coupling system at a rail joint. *Proc Inst Mech Eng Part F J Rail Rapid Transit.* 2014 Oct 12;229(4):364–74.
29. García AO. *Numerical and experimental analysis of the vertical dynamic behaviour of a railway track.* MSc Thesis, Delft University of Technology; 2014.
30. NR/L2/TRK/030 ISSUE 4:2016. Concrete sleepers and bearers.
31. Andersson A, Berglund H, Blomberg J et al. *The Influence of Stiffness Variations in Railway Tracks.* Bachelor Thesis, Chalmers University of Technology; 2013.
32. Grossoni I, Andrade AR, Bezin Y. Assessing the role of longitudinal variability of vertical track stiffness in the long-term deterioration. *IAVSD 24th International Symposium on Dynamics of Vehicles on Roads and Tracks*, Graz, Austria, 17-21 August 2015.
33. Steffens DM. *Identification and development of a model of railway track dynamic behaviour.* MEng Thesis, Queensland University of Technology; 2005.
34. Sun YQ, Cole C, Kerr M et al. Use of Simulations in Determination of Wheel Impact Forces P1 and P2 Due to Rail Dip Defects. In: *AusRAIL PLUS 2009*, Adelaide, Australia, 17-19 November 2009.